Article

# Non-ionotropic NMDA receptor signaling alters structural plasticity of dendritic spines in a mouse model of schizophrenia

**Deborah K. Park[1], Ivar S. Stein[1], Eden V. Barragan[1,2], John A. Gray[1,2], Karen Zito[1,*]**

[1]Center for Neuroscience
[2]Department of Neurology
University of California, Davis, CA 95618, USA.

[*]Correspondence should be addressed to Karen Zito, Center for Neuroscience, University of California Davis, Davis, CA, 95618 USA. Tel: 530-752-7832; e-mail: kzito@ucdavis.edu.

Running title: Non-ionotropic NMDAR signaling in schizophrenia

## Abstract

Schizophrenia is a psychiatric disorder that affects over 20 million people globally. Notably, schizophrenia is associated with decreased density of dendritic spines and decreased levels of D-serine, a co-agonist of the *N*-methyl-D-aspartate receptor (NMDAR), and hypofunction of NMDARs is thought to play a role in the pathophysiology of schizophrenia. We hypothesized that lowered D-serine levels associated with schizophrenia would bias toward ion flux-independent signaling by the NMDAR, which drives spine shrinkage and loss. Using a schizophrenia mouse model lacking the enzyme for D-serine production (serine racemase knock out; SRKO), we show that activity-dependent spine growth is inhibited in SRKO mice but can be acutely rescued by exogenous D-serine. When examining a wider range of stimulus strengths, we observed activity-dependent spine growth at higher stimulus strengths, but overall found a strong bias toward spine shrinkage in the SRKO mice as compared to wild-type littermates. Furthermore, we demonstrate that enhanced ion flux-independent signaling through the NMDAR contributes to this bias toward spine shrinkage, which is likely exacerbated by an increase in synaptic NMDARs in hippocampal synapses of SRKO mice. Our results support a model in which the lowered D-serine levels associated with schizophrenia lead to increased ion flux-independent NMDAR signaling and a bias toward spine shrinkage that could play an important role in the loss of dendritic spines associated with schizophrenia.

## Introduction

Experience-dependent growth and long-term stabilization of dendritic spines are critical for learning and memory formation (1-3). These spine structural changes are tightly associated with long-term potentiation (LTP) (4) and long-term depression (LTD) (5, 6) of synaptic strength and are mediated through *N*-methyl-D-aspartate receptors (NMDARs). NMDARs open to allow influx of calcium upon the binding of glutamate and co-agonist, glycine or D-serine, and they also signal in an ion flux-independent manner upon the binding of glutamate alone (7-10). Notably, ion-flux independent (non-ionotropic) NMDAR signaling mediates LTD and spine shrinkage, and is also critical for LTP-induced spine growth (11).

Dysfunctional NMDAR signaling is thought to contribute to the etiology of schizophrenia, a psychiatric disorder that affects up to 1% of the global population and is characterized by a variety of symptoms such as hallucinations and cognitive deficits (12). These debilitating symptoms may be linked to synaptic and neuroanatomical changes in the brain, such as decreased spine densities (13, 14). As NMDARs mediate bidirectional structural plasticity and stabilization of spines (11, 15), alterations in NMDAR function influence spine densities (16-18) and impact the ability to learn and form memories (19). Notably, patients have decreased levels of D-serine (20, 21) and elevated levels of the endogenous NMDAR co-agonist blocker, kynurenic acid (22), and the enzyme for D-serine production is a risk genes for schizophrenia (12). Importantly, animal studies that mimic NMDAR hypofunction by reducing co-agonist binding or ion flux produce both cognitive deficits and decreased spine density similar to those associated with schizophrenia (23-27).

We hypothesized that the decreased D-serine level associated with schizophrenia promotes ion flux-independent NMDAR signaling (7, 9), creating a bias for spine shrinkage and ultimately leading to decreased spine density. To test our hypothesis, we used a schizophrenia mouse model, serine racemase knockout (SRKO) (23), which lacks the enzyme required for D-serine production. Similar to patients with schizophrenia, these mutant mice have decreased levels of D-serine, decreased spine densities and cognitive deficits (23, 28). We found that SRKO mice have impaired activity-dependent spine growth, and that activity-dependent spine structural plasticity is biased toward spine shrinkage. Furthermore, we observed increased numbers of synaptic NMDARs, reduced CaMKII activation, and increased non-ionotropic NMDAR signaling at hippocampal synapses of SRKO animals. Our study supports a model in which decreased D-serine levels lead to increased ion flux-independent NMDAR signaling that promotes spine shrinkage and drives decreased spine densities associated with schizophrenia.

## Materials and methods

### Animals

SRKO (23) and GFP-M (29) mice in a C57BL/6J background were crossed to generate serine racemase knockout and wild-type mice with a GFP cell fill in a subset of CA1 hippocampal pyramidal neurons. All experimental protocols were approved by the University of California Davis Institutional Animal Care and Use Committee.

### Two-photon imaging and uncaging

Acute hippocampal slices were prepared from P14-21 WT and SRKO littermates of both sexes as described (11). GFP-expressing CA1 pyramidal neurons at depths of 10-50 µm were imaged using a custom two-photon microscope (30). For each neuron, image stacks (512 × 512 pixels; 0.02 µm per pixel; 1-µm z-steps) were collected from one segment of secondary or tertiary basal dendrite at 5 min intervals at 27-30 °C in recirculating artificial cerebral spinal fluid (ACSF; in mM: 127 NaCl, 25 $NaHCO_3$, 1.2 $NaH_2PO_4$, 2.5 KCl, 25 D-glucose, aerated with 95%$O_2$/5%$CO_2$, ~310 mOsm, pH 7.2) with 1 µM TTX, 0.1 mM $Mg^{2+}$, and 2 mM $Ca^{2+}$, unless otherwise stated. Cells were pre-incubated for at least 10 min with 10 µM D-serine (Tocris) or for at least 30 min with 10 µM L-689,560 (L-689, Tocris) and 10 µM Bay-K (Tocris), which were included as indicated. Images are maximum projections of three-dimensional image stacks after applying a median filter (3 × 3) to raw image data.

High-frequency uncaging (HFU) consisted of 60 pulses (720 nm; 2 ms duration, 7-11 mW at the sample) at 2 Hz delivered in ACSF containing (in mM): 2 $Ca^{2+}$, 0.1 $Mg^{2+}$, 2.5 MNI-glutamate, and 0.001 TTX. The beam was parked at a point ~0.5-1 µm from the spine at the position farthest from the dendrite. HFU+ stimulation consisted of 60 pulses (720 nm; 8 ms duration, ~6-10 mW at the sample) at 6 Hz, delivered in ACSF containing (in mM): 10 $Ca^{2+}$, 0.1 $Mg^{2+}$, 5 MNI-glutamate, and 0.001 TTX. For the imaging experiment involving HFU+ stimulation, healthy and stimulus responsive cells were selected as described (11).

Estimated spine volume was measured from background-subtracted green fluorescence using the integrated pixel intensity of a boxed region surrounding the spine head, as described (30). Statistical comparisons were made with Student's t-test.

### Electrophysiology

Modified transverse 300 µm slices of dorsal hippocampus were prepared from P15–P19 mice anesthetized with isoflurane, as described (31), and mounted cut side down on a Leica VT1200 vibratome in ice-cold sucrose cutting buffer containing (in mM): 210 sucrose, 25 $NaHCO_3$, 2.5

KCl, 1.25 $NaH_2PO_4$, 7 glucose, 7 $MgCl_2$, and 0.5 $CaCl_2$. Slices were recovered for 1 h in 32°C ACSF solution containing (in mM): 119 NaCl, 26.2 $NaHCO_3$, 11 glucose, 2.5 KCl, 1 NaH2PO4, 2.5 $CaCl_2$, and 1.3 $MgSO_4$.

Slices were transferred to a submersion chamber and perfused in room temperature ACSF containing picrotoxin (0.1 mM) and TTX (0.5 μM) and saturated with 95%$O_2$/5%$CO_2$. mEPSCs were recorded from CA1 pyramidal neurons patched with 3–5 MΩ borosilicate pipettes filled with intracellular solution containing (in mM): 135 cesium methanesulfonate, 8 NaCl, 10 HEPES, 0.3 Na-GTP, 4 Mg-ATP, 0.3 EGTA, and 5 QX-314 (290 mOsm, pH 7.3). Series resistance was monitored and not compensated. Cells were discarded if series resistance varied by more than 25%. Recordings were obtained with a MultiClamp 700B amplifier (Molecular Devices), filtered at 2 kHz, digitized at 10 Hz.

Miniature synaptic events were analyzed using Mini Analysis software (Synaptosoft) using a threshold amplitude of 5 pA for peak detection. To generate cumulative probability plots for amplitude and inter-event time interval, events from each CA1 pyramidal neuron (>100 per cell) were pooled for each group. The Kolmogorov-Smirnov two-sample test (KS test) was used to compare the distribution of events between WT and SRKO. Statistical comparisons were made with Student's unpaired t-test, using Graphpad Prism 8.0 (Graphpad Software).

**Biochemistry**

Hippocampi of P20 mice of either sex were homogenized with 1% deoxycholate. For immunoprecipitation, 50 μL of Protein G Dynabeads (Invitrogen) were pre-incubated with 2.4 μg of either CaMKIIα (32-34) or mouse IgG antibody (sc-2025, Santa Cruz Biotechnology) at RT for 10 min, washed with 0.05% TBS-tween, incubated with 1000-1500 μg of protein lysate for 30 min at RT, washed four times with 0.01% TBS-triton, and then eluted. For PSD isolation, lysates were fractionated by centrifugation and sucrose gradient, and extracted with Triton X-100, as described (35).

Protein samples were run on a SDS-PAGE gel at 30 mA and transferred to 0.45 um PVDF membrane for 210 min at 50 V. Blots were stained for total protein with Revert 700 Total Protein Stain Kit (LICOR). Membranes were blocked with TBS Odyssey Blocking Buffer (LICOR) and incubated overnight at 4°C with primary antibodies for GluN2B, GluN2A, GluN1, CaMKIIα (32-34), pT286 CaMKIIα (sc-12886R, Santa Cruz), synaptophysin (Sigma S5768), or serine racemase (sc-365217, Santa Cruz). Secondary antibody (IRDye; LICOR) incubation was for 1 h at RT and the blots scanned and analyzed using Odyssey CLx and Image Studio. Statistical comparisons were made with Student's unpaired t-test.

### Statistical analysis

Cells for each condition were obtained from at least 3 independent hippocampal acute slices preparations of both sexes. Data analysis was done blind to the experimental condition. All statistics were calculated across cells. All data are represented as mean ± standard error of the mean (SEM). Statistical significance was set at $p < 0.05$ (two-tailed t test).

## Results

### LTP-associated growth of dendritic spines is impaired in SRKO mice

NMDAR-dependent LTP and associated spine growth, mediated by simultaneous binding of glutamate and synaptic co-agonist, D-serine, is an important cellular process for memory formation and maintenance of spine density (1, 15, 36). Based on the requirement for robust calcium influx during NMDAR-dependent spine growth and stabilization, we hypothesized that reduced bioavailability of D-serine observed in patients with schizophrenia (20, 21) would obstruct LTP-associated spine growth and instead result in spine destabilization and the reduced spine density associated with the disorder (13, 14).

To test our hypothesis, we crossed the SRKO mouse model of schizophrenia (23) with the GFP-M (29) mouse line to obtain D-serine deficient mice that have sparse neuronal GFP expression in the hippocampus allowing visualization of dendrites and spines. High-frequency uncaging (HFU) of glutamate at single dendritic spines on basal dendrites of CA1 neurons resulted in long-term growth of WT, but not SRKO spines (**Fig. 1A-C**). Notably, the lack of long-term spine growth in SRKO was rescued with acute treatment of 10 μM D-serine (**Fig. 1D-F**), demonstrating that the deficit in long-term spine growth is not due to chronic alterations in the SRKO animals or a role for serine racemase other than its role in synthesis of D-serine. Thus, LTP-associated spine growth is impaired in SRKO mice, as expected, and in line with the previously reported observation of LTP deficit in these mice (23).

### Structural plasticity curve is shifted to favor spine shrinkage in SRKO mice

Upon observing a complete block of activity-dependent spine growth in the SRKO mice, we wondered whether this result was indicative of a complete inability to support spine structural plasticity in the SRKO, or whether a stronger stimulus might be sufficient to overcome the impairment of LTP-associated spine growth in the SRKO. To test this, we increased the extracellular $Ca^{2+}$ concentration to 5 mM in order to strengthen the influx of $Ca^{2+}$ in response to HFU stimulation. We found that HFU in 5 mM $CaCl_2$ led to long-term spine growth for both WT

and SRKO (**Fig. 2A, B**), demonstrating that the signaling mechanisms downstream of $Ca^{2+}$ influx that support long-term spine growth are intact in SRKO.

We next wondered whether SRKO mice exhibit an overall bias for spine shrinkage across a broad range of stimulus strengths. Notably, although HFU normally leads to spine growth, this LTP-inducing stimulation can instead lead to spine shrinkage in the absence of co-agonist binding and strong influx of $Ca^{2+}$, due to glutamate-induced, ion flux-independent signaling of the NMDAR (9). By delivering HFU across a broad range of $CaCl_2$ concentrations, we probed for bias in the direction of spine structural plasticity in SRKO mice relative to WT. Plotting the spine volume change at various $CaCl_2$ concentrations should produce an S-shaped plasticity curve that depicts spine shrinkage turning into growth as the $CaCl_2$ concentration increases. A bias for growth should result in the structural plasticity curve of SRKO shifting leftward relative to the WT, whereas a bias for shrinkage would result in a shift to the right.

We found that HFU in 3 mM $CaCl_2$ also causes spines of both WT and SRKO to undergo growth as non-ionotropic NMDAR signaling is still paired with sufficient amount of $Ca^{2+}$ influx for growth to occur (**Fig. 2C, D**). In contrast, HFU in 1.5 mM $CaCl_2$ leads to spine shrinkage in SRKO while WT does not undergo any structural change (**Fig. 2E, F**). Finally, HFU in 0.3 mM $CaCl_2$ causes both WT and SRKO spines to undergo shrinkage as non-ionotropic NMDAR signaling occurs with minimal amounts of calcium influx (**Fig. 2G, H**). Plotting this data together with our results from Figure 1, we observe that both genotypes have similar S-shaped plasticity curves, but the SRKO structural plasticity curve is shifted to the right (**Fig. 2I**). The rightward shift in the plasticity curve of SRKO mice supports that there is a bias for spine shrinkage in the SRKO as compared to WT.

**Increased synaptic NMDARs and decreased CaMKII activation in SRKO**

Because elevated NMDAR expression has been observed in SRKO (37, 38), we wondered if this was also the case in the hippocampus in young mice and thus, in combination with the reduction in D-serine levels, would allow for even more non-ionotropic NMDAR signaling during glutamatergic signaling. We hypothesized that the bias for spine shrinkage in SRKO may be due to the combination of reduced D-serine levels and increased expression of NMDARs available for non-ionotropic NMDAR signaling.

To investigate whether SRKO mice have more NMDARs at dendritic spines within the hippocampus, we isolated PSD fractions of P20 SRKO mice. We found an increased band intensity in SRKO for obligatory subunit GluN1, suggesting greater number of synaptic NMDARs in SRKO animals (**Fig. 3A, B**). Interestingly, we also observed increased synaptic enrichment

(**Fig. 3A, B**) and total expression (**Fig. 3C, D**) of GluN2B in SRKO relative to WT. Despite the greater number of NMDARs, we expected disrupted calcium-dependent downstream signaling due to reduced co-agonist binding and thus reduction of calcium influx through the NMDAR. Indeed, when we probed CaMKII-GluN2B interaction by immunoprecipitation and for phosphorylation of CaMKII at the T286 autophosphorylation site, which are both integral for LTP and indicative of strong calcium influx (39, 40), we found that basal levels of CaMKII-GluN2B interaction and pT286 are both decreased in SRKO (**Fig. 3E, F**), despite no change in CaMKII expression or enrichment levels in SRKO (**Fig. 3A, B**), supporting decreased NMDAR calcium-dependent downstream signaling in these mutant mice.

**Enhanced non-ionotropic NMDAR signaling in SRKO mice**

Our observations of increased number of synaptic NMDARs in mice with reduced D-serine levels support that altered structural plasticity in SRKO could be due to increased non-ionotropic NMDAR signaling driven by glutamate binding to the increased number of NMDARs, in the absence of co-agonist binding (41). Notably, non-ionotropic NMDAR signaling is required not only for spine shrinkage, but also for spine growth, which occurs in the presence of strong $Ca^{2+}$ influx (11). Because there is no direct means of measuring the relative amount of non-ionotropic signaling, we set out to probe the relative contribution of non-ionotropic NMDAR signaling to spine structural plasticity between the SRKO and WT in an assay that combines non-ionotropic signaling through the NMDAR with independently increased calcium influx through voltage-gated calcium channels (VGCCs) to drive spine growth (**Fig. 4A**). We speculated that we would see enhanced spine growth in the SRKO due to the enhanced numbers of NMDARs driving more glutamate-induced non-ionotropic NMDAR signaling (**Fig. 4A**).

To isolate non-ionotropic NMDAR signaling in SRKO mice, we used the NMDAR co-agonist site inhibitor L-689,560 (L-689) to mimic the absence of co-agonist and thus block NMDAR-mediated $Ca^{2+}$ influx following glutamate binding. We combined this with the L-type $Ca^{2+}$ channel agonist Bay K 8644 (Bay K) to promote $Ca^{2+}$ influx through voltage-gated calcium channels (VGCCs). A modified HFU paradigm (HFU+) of higher frequency and longer duration stimuli was used to ensure strong AMPAR-dependent depolarization of the spine for VGCC opening, adjusted to induce a smaller, non-saturated increase in long-term spine size in WT (**Fig. 4B-D**). Remarkably, this same HFU+ stimulation drove a robust increase in spine growth in SRKO mice (**Fig. 4B-D**). This enhancement in spine growth was not due to increased AMPAR function in SRKO mice, as the amplitude of miniature excitatory postsynaptic currents (mEPSCs) was not different between WT and SRKO (**Fig. 4E**). As the amount of AMPAR-

mediated depolarization and thus VGCC opening between the two genotypes should be of comparable level, we interpret the greater amount of spine growth in SRKO to be indicative of a higher level of non-ionotropic NMDAR signaling. These results support our model (**Fig. 4F**) in which increased synaptic NMDARs in conditions of reduced D-serine levels in SRKO lead to more non-ionotropic NMDAR signaling that creates a bias toward spine shrinkage and loss.

## Discussion

### Lowered D-serine levels create a bias towards spine shrinkage

It has been widely reported that schizophrenia is associated with a reduction in dendritic spine density that is thought to contribute to cognitive deficits. As changes in spine density and gray matter volume mirror each other (42), and longitudinal MRI studies of high risk individuals report normal increase in gray matter during childhood that then declines in adolescence (43-45), a time when spine pruning increases (46), it has been suggested that excessive spine elimination, rather than a deficit in new spine outgrowth, is the potential cause of decreased spine density in schizophrenia (47).

Here, we show a disruption of long-term spine growth and a bias toward activity-induced spine shrinkage in the SRKO mouse model of schizophrenia, which is reported to have decreased spine density at older ages (28). Although we observed a shift in the plasticity curve for the SRKO, we were able to induce both spine shrinkage and growth, and it has been demonstrated that spine density can be rescued in these mice with D-serine treatment (48). Thus, our studies support that serine racemase, the enzyme that produces D-serine and observed to interact with various synaptic structural proteins such as PSD95 (49, 50), is itself not required for structural plasticity of spines. Notably, D-serine has been shown to promote spine stability (49), likely through increased incidence of simultaneous glutamate and co-agonist binding to the NMDAR for $Ca^{2+}$ influx required for stabilization (15). As glutamate binding alone to the NMDAR drives spine shrinkage in an ion-flux independent manner (9), we propose that the enhancement of non-ionotropic NMDAR signaling due to the decreased levels of D-serine biases toward spine shrinkage in the SRKO mice and may subsequently drive the spine loss associated with schizophrenia.

### Enhanced levels and altered composition of synaptic NMDARs in SRKO mice

Our observation of increased synaptic enrichment of NMDARs relative to WT within the hippocampus is expected based on previous studies on SRKO mice showing increased expression of GluN1 (37, 38) and GluN2B (23, 51). These changes in the overall number and

composition of NMDARs are likely to be the consequence of lack of D-serine, as prior studies have demonstrated the role of co-agonist binding in priming of the NMDAR for endocytosis, with D-serine specifically acting on GluN2B subunits (52, 53). In addition, we found that this increase in the number of NMDARs led to an increase in the magnitude of non-ionotropic signaling in SRKO, which would be expected to drive enhanced spine loss (11).

Notably, despite the enhancement of NMDAR levels at the synapse, we observed decreased CaMKII-GluN2B interaction and decreased autophosphorylation of CaMKII in SRKO mice, which we attribute to the lack of strong $Ca^{2+}$ influx required for increasing both CaMKII activity and interaction to GluN2B (54). This altered downstream CaMKII signaling likely contributes to NMDAR hypofunction in schizophrenia (55).

**Enhanced non-ionotropic NMDAR signaling in SRKO mice**

We made several observations that support our hypothesis that there is increased ion flux-independent NMDAR signaling driving spine destabilization in the SRKO mice. First, we observed that stimulation protocols which normally induce spine growth in WT mice can instead drives spine shrinkage in SRKO. Second, we found increased NMDARs at hippocampal synapses in the SRKO mice, which, in combination with the reduced D-serine levels, would further bias NMDARs toward ion flux-independent signaling. Finally, we showed that supplementing non-ionotropic NMDAR activation with $Ca^{2+}$ influx from voltage-gated $Ca^{2+}$ channel leads to more spine growth in SRKO than in WT, supporting increased ion flux-independent NMDAR signaling in these animals. This enhanced non-ionotropic NMDAR signaling would be expected to drive enhanced spine shrinkage and eventual spine elimination.

Notably, studies in which uncompetitive antagonists of NMDARs produce schizophrenia like symptoms in healthy individuals and exacerbate them in patients with the disorder helped give rise to the NMDAR hypofunction hypothesis (56-59). Due to high sensitivity of inhibitory GABAergic neurons to NMDAR blockers (60, 61), decreased expression of interneurons (62-64), and GABAergic markers (65-68), NMDAR hypofunction caused by reduced D-serine levels in schizophrenia may lead to disinhibition of excitatory neurons and result in glutamate spillover (69-72). Indeed, SRKO mice have been observed to have decreased PV expression and altered excitatory/inhibitory balance from GABAergic dysfunction (73-75). This disinhibition should result in greater release of glutamate at dendritic spines that, when paired with reduced D-serine levels, would increase the amount of non-ionotropic NMDAR activation even further to promote spine shrinkage (41) and decrease in spine density in the SRKO and schizophrenia (13, 14, 28).

## Conclusion

Here we show that the SRKO mouse model of schizophrenia displays altered dendritic structural plasticity that biases toward spine shrinkage. We further report an increased number of synaptic NMDARs in the hippocampus of the SRKO mice and increased ion flux-independent NMDAR signaling at hippocampal spines. Taken together, our findings support a model in which NMDAR hypofunction brought on by lack of D-serine, promotes increased NMDAR expression and excessive non-ionotropic NMDAR signaling that drives a bias towards spine shrinkage and likely contributes to decreased spine density associated with schizophrenia.

## Acknowledgements

This work was supported by the NIH R01 NS062736 (K.Z.), R01 MH117130 (J.A.G.), T32GM099608 (E.V.B.), and by an ARCS scholar award (D.K.P.). We thank Joseph Coyle for the SRKO mice; Johannes Hell for CaMKIIα, GluN1, GluN2B, and GluN2A antibodies; Julie Culp, Jennifer Jahncke, and Lorenzo Tom for support with experiments and analysis; and Joseph Coyle, Scott Cameron, and Samuel Petshow for critical reading of the manuscript.

## Author contributions

D.K.P., I.S.S., and K.Z. designed the study and wrote the manuscript. D.K.P. performed the imaging and biochemistry experiments and analysis. J.A.G. and E.V.B. designed and E.V.B. performed the electrophysiology experiments and analysis. All authors edited the manuscript.

## Conflict of interest

The authors declare no competing interests.

## References


1. Hayashi-Takagi A, Yagishita S, Nakamura M, Shirai F, Wu YI, Loshbaugh AL, et al. Labelling and optical erasure of synaptic memory traces in the motor cortex. Nature. 2015;525(7569):333-8.
2. Yang G, Pan F, Gan WB. Stably maintained dendritic spines are associated with lifelong memories. Nature. 2009;462(7275):920-4.
3. Xu T, Yu X, Perlik AJ, Tobin WF, Zweig JA, Tennant K, et al. Rapid formation and selective stabilization of synapses for enduring motor memories. Nature. 2009;462(7275):915-9.
4. Matsuzaki M, Honkura N, Ellis-Davies GC, Kasai H. Structural basis of long-term potentiation in single dendritic spines. Nature. 2004;429(6993):761-6.
5. Zhou Q, Homma KJ, Poo MM. Shrinkage of dendritic spines associated with long-term depression of hippocampal synapses. Neuron. 2004;44(5):749-57.
6. Oh WC, Hill TC, Zito K. Synapse-specific and size-dependent mechanisms of spine structural plasticity accompanying synaptic weakening. Proc Natl Acad Sci U S A. 2013;110(4):E305-12.
7. Nabavi S, Kessels HW, Alfonso S, Aow J, Fox R, Malinow R. Metabotropic NMDA receptor function is required for NMDA receptor-dependent long-term depression. Proc Natl Acad Sci U S A. 2013;110(10):4027-32.
8. Dore K, Aow J, Malinow R. Agonist binding to the NMDA receptor drives movement of its cytoplasmic domain without ion flow. Proc Natl Acad Sci U S A. 2015;112(47):14705-10.
9. Stein IS, Gray JA, Zito K. Non-Ionotropic NMDA Receptor Signaling Drives Activity-Induced Dendritic Spine Shrinkage. The Journal of neuroscience : the official journal of the Society for Neuroscience. 2015;35(35):12303-8.
10. Wong JM, Gray JA. Long-Term Depression Is Independent of GluN2 Subunit Composition. The Journal of neuroscience : the official journal of the Society for Neuroscience. 2018;38(19):4462-70.
11. Stein IS, Park DK, Claiborne N, Zito K. Non-ionotropic NMDA receptor signaling gates bidirectional structural plasticity of dendritic spines. Cell Rep. 2021;34(4):108664.
12. Coyle JT. Schizophrenia: Basic and Clinical. Adv Neurobiol. 2017;15:255-80.
13. Rosoklija G, Toomayan G, Ellis SP, Keilp J, Mann JJ, Latov N, et al. Structural abnormalities of subicular dendrites in subjects with schizophrenia and mood disorders: preliminary findings. Arch Gen Psychiatry. 2000;57(4):349-56.
14. Sweet RA, Henteleff RA, Zhang W, Sampson AR, Lewis DA. Reduced dendritic spine density in auditory cortex of subjects with schizophrenia. Neuropsychopharmacology. 2009;34(2):374-89.
15. Hill TC, Zito K. LTP-induced long-term stabilization of individual nascent dendritic spines. The Journal of neuroscience : the official journal of the Society for Neuroscience. 2013;33(2):678-86.
16. Ultanir SK, Kim JE, Hall BJ, Deerinck T, Ellisman M, Ghosh A. Regulation of spine morphology and spine density by NMDA receptor signaling in vivo. Proc Natl Acad Sci U S A. 2007;104(49):19553-8.
17. Alvarez VA, Ridenour DA, Sabatini BL. Distinct structural and ionotropic roles of NMDA receptors in controlling spine and synapse stability. J Neurosci. 2007;27(28):7365-76.

18. Brigman JL, Wright T, Talani G, Prasad-Mulcare S, Jinde S, Seabold GK, et al. Loss of GluN2B-containing NMDA receptors in CA1 hippocampus and cortex impairs long-term depression, reduces dendritic spine density, and disrupts learning. J Neurosci. 2010;30(13):4590-600.

19. Kannangara TS, Eadie BD, Bostrom CA, Morch K, Brocardo PS, Christie BR. GluN2A-/- Mice Lack Bidirectional Synaptic Plasticity in the Dentate Gyrus and Perform Poorly on Spatial Pattern Separation Tasks. Cereb Cortex. 2015;25(8):2102-13.

20. Bendikov I, Nadri C, Amar S, Panizzutti R, De Miranda J, Wolosker H, et al. A CSF and postmortem brain study of D-serine metabolic parameters in schizophrenia. Schizophr Res. 2007;90(1-3):41-51.

21. Hashimoto K, Shimizu E, Komatsu N, Watanabe H, Shinoda N, Nakazato M, et al. No changes in serum epidermal growth factor levels in patients with schizophrenia. Psychiatry Res. 2005;135(3):257-60.

22. Plitman E, Iwata Y, Caravaggio F, Nakajima S, Chung JK, Gerretsen P, et al. Kynurenic Acid in Schizophrenia: A Systematic Review and Meta-analysis. Schizophr Bull. 2017;43(4):764-77.

23. Basu AC, Tsai GE, Ma CL, Ehmsen JT, Mustafa AK, Han L, et al. Targeted disruption of serine racemase affects glutamatergic neurotransmission and behavior. Mol Psychiatry. 2009;14(7):719-27.

24. Barnes SA, Sawiak SJ, Caprioli D, Jupp B, Buonincontri G, Mar AC, et al. Impaired limbic cortico-striatal structure and sustained visual attention in a rodent model of schizophrenia. Int J Neuropsychopharmacol. 2014;18(2).

25. Latysheva NV, Raevskii KS. Behavioral analysis of the consequences of chronic blockade of NMDA-type glutamate receptors in the early postnatal period in rats. Neurosci Behav Physiol. 2003;33(2):123-31.

26. Wu H, Wang X, Gao Y, Lin F, Song T, Zou Y, et al. NMDA receptor antagonism by repetitive MK801 administration induces schizophrenia-like structural changes in the rat brain as revealed by voxel-based morphometry and diffusion tensor imaging. Neuroscience. 2016;322:221-33.

27. Schobel SA, Chaudhury NH, Khan UA, Paniagua B, Styner MA, Asllani I, et al. Imaging patients with psychosis and a mouse model establishes a spreading pattern of hippocampal dysfunction and implicates glutamate as a driver. Neuron. 2013;78(1):81-93.

28. Balu DT, Li Y, Puhl MD, Benneyworth MA, Basu AC, Takagi S, et al. Multiple risk pathways for schizophrenia converge in serine racemase knockout mice, a mouse model of NMDA receptor hypofunction. Proc Natl Acad Sci U S A. 2013;110(26):E2400-9.

29. Feng G, Mellor RH, Bernstein M, Keller-Peck C, Nguyen QT, Wallace M, et al. Imaging neuronal subsets in transgenic mice expressing multiple spectral variants of GFP. Neuron. 2000;28(1):41-51.

30. Woods GF, Oh WC, Boudewyn LC, Mikula SK, Zito K. Loss of PSD-95 enrichment is not a prerequisite for spine retraction. The Journal of neuroscience : the official journal of the Society for Neuroscience. 2011;31(34):12129-38.

31. Bischofberger J, Engel D, Li L, Geiger JR, Jonas P. Patch-clamp recording from mossy fiber terminals in hippocampal slices. Nat Protoc. 2006;1(4):2075-81.

32. Leonard AS, Davare MA, Horne MC, Garner CC, Hell JW. SAP97 is associated with the alpha-amino-3-hydroxy-5-methylisoxazole-4-propionic acid receptor GluR1 subunit. J Biol Chem. 1998;273(31):19518-24.

33. Leonard AS, Lim IA, Hemsworth DE, Horne MC, Hell JW. Calcium/calmodulin-dependent protein kinase II is associated with the N-methyl-D-aspartate receptor. Proc Natl Acad Sci U S A. 1999;96(6):3239-44.

34. Lu Y, Allen M, Halt AR, Weisenhaus M, Dallapiazza RF, Hall DD, et al. Age-dependent requirement of AKAP150-anchored PKA and GluR2-lacking AMPA receptors in LTP. EMBO J. 2007;26(23):4879-90.

35. Dosemeci A, Tao-Cheng JH, Vinade L, Jaffe H. Preparation of postsynaptic density fraction from hippocampal slices and proteomic analysis. Biochem Biophys Res Commun. 2006;339(2):687-94.

36. Kwon HB, Sabatini BL. Glutamate induces de novo growth of functional spines in developing cortex. Nature. 2011;474(7349):100-4.

37. Mustafa AK, Ahmad AS, Zeynalov E, Gazi SK, Sikka G, Ehmsen JT, et al. Serine racemase deletion protects against cerebral ischemia and excitotoxicity. J Neurosci. 2010;30(4):1413-6.

38. Balu DT, Coyle JT. Glutamate receptor composition of the post-synaptic density is altered in genetic mouse models of NMDA receptor hypo- and hyperfunction. Brain Res. 2011;1392:1-7.

39. Halt AR, Dallapiazza RF, Zhou Y, Stein IS, Qian H, Juntti S, et al. CaMKII binding to GluN2B is critical during memory consolidation. EMBO J. 2012;31(5):1203-16.

40. Lee SJ, Escobedo-Lozoya Y, Szatmari EM, Yasuda R. Activation of CaMKII in single dendritic spines during long-term potentiation. Nature. 2009;458(7236):299-304.

41. Stein IS, Park DK, Flores JC, Jahncke JN, Zito K. Molecular Mechanisms of Non-ionotropic NMDA Receptor Signaling in Dendritic Spine Shrinkage. The Journal of neuroscience : the official journal of the Society for Neuroscience. 2020;40(19):3741-50.

42. Bennett MR. Schizophrenia: susceptibility genes, dendritic-spine pathology and gray matter loss. Prog Neurobiol. 2011;95(3):275-300.

43. Thompson PM, Vidal C, Giedd JN, Gochman P, Blumenthal J, Nicolson R, et al. Mapping adolescent brain change reveals dynamic wave of accelerated gray matter loss in very early-onset schizophrenia. Proc Natl Acad Sci U S A. 2001;98(20):11650-5.

44. Job DE, Whalley HC, Johnstone EC, Lawrie SM. Grey matter changes over time in high risk subjects developing schizophrenia. Neuroimage. 2005;25(4):1023-30.

45. Pantelis C, Velakoulis D, McGorry PD, Wood SJ, Suckling J, Phillips LJ, et al. Neuroanatomical abnormalities before and after onset of psychosis: a cross-sectional and longitudinal MRI comparison. Lancet. 2003;361(9354):281-8.

46. Penzes P, Cahill ME, Jones KA, VanLeeuwen JE, Woolfrey KM. Dendritic spine pathology in neuropsychiatric disorders. Nature neuroscience. 2011;14(3):285-93.

47. Glausier JR, Lewis DA. Dendritic spine pathology in schizophrenia. Neuroscience. 2013;251:90-107.

48. Balu DT, Coyle JT. Chronic D-serine reverses arc expression and partially rescues dendritic abnormalities in a mouse model of NMDA receptor hypofunction. Neurochem Int. 2014;75:76-8.

49. Lin H, Jacobi AA, Anderson SA, Lynch DR. D-Serine and Serine Racemase Are Associated with PSD-95 and Glutamatergic Synapse Stability. Front Cell Neurosci. 2016;10:34.

50. Ma TM, Paul BD, Fu C, Hu S, Zhu H, Blackshaw S, et al. Serine racemase regulated by binding to stargazin and PSD-95: potential N-methyl-D-aspartate-alpha-amino-3-hydroxy-5-methyl-4-isoxazolepropionic acid (NMDA-AMPA) glutamate neurotransmission cross-talk. J Biol Chem. 2014;289(43):29631-41.

51. Wong JM, Folorunso OO, Barragan EV, Berciu C, Harvey TL, Coyle JT, et al. Postsynaptic Serine Racemase Regulates NMDA Receptor Function. J Neurosci. 2020;40(50):9564-75.

52. Nong Y, Huang YQ, Ju W, Kalia LV, Ahmadian G, Wang YT, et al. Glycine binding primes NMDA receptor internalization. Nature. 2003;422(6929):302-7.

53. Ferreira JS, Papouin T, Ladepeche L, Yao A, Langlais VC, Bouchet D, et al. Co-agonists differentially tune GluN2B-NMDA receptor trafficking at hippocampal synapses. Elife. 2017;6.

54. Goodell DJ, Zaegel V, Coultrap SJ, Hell JW, Bayer KU. DAPK1 Mediates LTD by Making CaMKII/GluN2B Binding LTP Specific. Cell Rep. 2017;19(11):2231-43.

55. Banerjee A, Wang HY, Borgmann-Winter KE, MacDonald ML, Kaprielian H, Stucky A, et al. Src kinase as a mediator of convergent molecular abnormalities leading to NMDAR hypoactivity in schizophrenia. Mol Psychiatry. 2015;20(9):1091-100.

56. Lahti AC, Weiler MA, Tamara Michaelidis BA, Parwani A, Tamminga CA. Effects of ketamine in normal and schizophrenic volunteers. Neuropsychopharmacology. 2001;25(4):455-67.

57. Newcomer JW, Farber NB, Jevtovic-Todorovic V, Selke G, Melson AK, Hershey T, et al. Ketamine-induced NMDA receptor hypofunction as a model of memory impairment and psychosis. Neuropsychopharmacology. 1999;20(2):106-18.

58. Javitt DC, Zukin SR. Recent advances in the phencyclidine model of schizophrenia. Am J Psychiatry. 1991;148(10):1301-8.

59. Krystal JH, Karper LP, Seibyl JP, Freeman GK, Delaney R, Bremner JD, et al. Subanesthetic effects of the noncompetitive NMDA antagonist, ketamine, in humans. Psychotomimetic, perceptual, cognitive, and neuroendocrine responses. Arch Gen Psychiatry. 1994;51(3):199-214.

60. Grunze HC, Rainnie DG, Hasselmo ME, Barkai E, Hearn EF, McCarley RW, et al. NMDA-dependent modulation of CA1 local circuit inhibition. J Neurosci. 1996;16(6):2034-43.

61. Homayoun H, Moghaddam B. NMDA receptor hypofunction produces opposite effects on prefrontal cortex interneurons and pyramidal neurons. J Neurosci. 2007;27(43):11496-500.

62. Hashimoto T, Arion D, Unger T, Maldonado-Aviles JG, Morris HM, Volk DW, et al. Alterations in GABA-related transcriptome in the dorsolateral prefrontal cortex of subjects with schizophrenia. Mol Psychiatry. 2008;13(2):147-61.

63. Hashimoto T, Volk DW, Eggan SM, Mirnics K, Pierri JN, Sun Z, et al. Gene expression deficits in a subclass of GABA neurons in the prefrontal cortex of subjects with schizophrenia. J Neurosci. 2003;23(15):6315-26.

64. Mellios N, Huang HS, Baker SP, Galdzicka M, Ginns E, Akbarian S. Molecular determinants of dysregulated GABAergic gene expression in the prefrontal cortex of subjects with schizophrenia. Biol Psychiatry. 2009;65(12):1006-14.

65. Glausier JR, Lewis DA. GABA and schizophrenia: Where we stand and where we need to go. Schizophr Res. 2017;181:2-3.

66. Gonzalez-Burgos G, Fish KN, Lewis DA. GABA neuron alterations, cortical circuit dysfunction and cognitive deficits in schizophrenia. Neural Plast. 2011;2011:723184.

67. Lewis DA, Hashimoto T, Morris HM. Cell and receptor type-specific alterations in markers of GABA neurotransmission in the prefrontal cortex of subjects with schizophrenia. Neurotox Res. 2008;14(2-3):237-48.

68. Lewis DA, Pierri JN, Volk DW, Melchitzky DS, Woo TU. Altered GABA neurotransmission and prefrontal cortical dysfunction in schizophrenia. Biol Psychiatry. 1999;46(5):616-26.

69. Gallinat J, McMahon K, Kuhn S, Schubert F, Schaefer M. Cross-sectional Study of Glutamate in the Anterior Cingulate and Hippocampus in Schizophrenia. Schizophr Bull. 2016;42(2):425-33.

70. Kraguljac NV, White DM, Reid MA, Lahti AC. Increased hippocampal glutamate and volumetric deficits in unmedicated patients with schizophrenia. JAMA Psychiatry. 2013;70(12):1294-302.

71. van Elst LT, Valerius G, Buchert M, Thiel T, Rusch N, Bubl E, et al. Increased prefrontal and hippocampal glutamate concentration in schizophrenia: evidence from a magnetic resonance spectroscopy study. Biol Psychiatry. 2005;58(9):724-30.

72. Lorrain DS, Baccei CS, Bristow LJ, Anderson JJ, Varney MA. Effects of ketamine and N-methyl-D-aspartate on glutamate and dopamine release in the rat prefrontal cortex: modulation by a group II selective metabotropic glutamate receptor agonist LY379268. Neuroscience. 2003;117(3):697-706.

73. Steullet P, Cabungcal JH, Coyle J, Didriksen M, Gill K, Grace AA, et al. Oxidative stress-driven parvalbumin interneuron impairment as a common mechanism in models of schizophrenia. Mol Psychiatry. 2017;22(7):936-43.

74. Ploux E, Bouet V, Radzishevsky I, Wolosker H, Freret T, Billard JM. Serine Racemase Deletion Affects the Excitatory/Inhibitory Balance of the Hippocampal CA1 Network. Int J Mol Sci. 2020;21(24).

75. Jami SA, Cameron S, Wong JM, Daly ER, McAllister AK, Gray JA. Increased excitation-inhibition balance due to a loss of GABAergic synapses in the serine racemase knockout model of NMDA receptor hypofunction. bioRxiv. 2020.

## Figure Legends

**Fig. 1 LTP-associated growth of dendritic spines is impaired in SRKO mice.**
**(A, D)** Representative images of basal dendrites of CA1 pyramidal neurons in acute hippocampal slices from of P14-21 WT and SRKO mice. Individual spines (yellow arrow) are stimulated with HFU of MNI-glutamate (yellow crosshair) during vehicle condition and in the presence of D-serine (10 μM). (**B, C)** HFU leads to growth in WT (black filled circles/bar; n=7 cells/7 mice; $p<0.05$) but not in SRKO (red filled circles/bar; n=9 cells/8 mice; $p=0.63$). Volume of unstimulated neighboring spines were not affected (open circles/bars). **(E, F)** Supplementing D-serine in SRKO (black filled circles/bar; n=6 cells/5 mice; $p<0.05$) rescues HFU-induced growth (red filled circles/bar; n=8 cells/7 mice; $p<0.05$). Data are represented as mean +/- SEM. *$p<0.05$; **$p<0.01$; ***$p<0.001$.

**Fig. 2 Structural plasticity is shifted to favor spine shrinkage in SRKO mice.**
**(A, B)** HFU in 5 mM $CaCl_2$ shows spine growth is saturated to comparable levels between WT (black filled circles/bar; n=7 cells/3 mice; $p<0.05$) and SRKO (red filled circles/bar; n=6 cells/2 mice; $p<0.05$). **(C, D)** HFU in 3 mM $CaCl_2$ allows for spine growth in both WT (black filled circles/bar; n=7 cells/5 mice; $p<0.05$) and SRKO (red filled circles/bar; n=9 cells/3 mice; $p<0.05$). **(E, F)** HFU in 1.5 mM $CaCl_2$ does not lead to any spine volume change in WT (black filled circles/bar; n=6 cells/6 mice; $p=0.13$) while shrinkage already occurs in SRKO (red filled circles/bar; n=8 cells/5 mice; $p<0.01$). **(G, H)** HFU in ACSF of 0.3 mM $CaCl_2$ leads to spine shrinkage in both WT (black filled circles/bar; n=7 cells/4 mice; $p<0.001$) and SRKO (red filled circles/bar; n=8 cells/5 mice; $p<0.001$). **(I)** Structural plasticity curve of SRKO mice is shifted to the right, demonstrating a bias for spine shrinkage over growth. Data are represented as mean +/- SEM. *$p<0.05$; **$p<0.01$; ***$p<0.001$.

**Fig. 3 Increased synaptic NMDARs and decreased CaMKII activation in SRKO.**
**(A, B)** PSD signals from P20 SRKO hippocampi (n=4 preps/12 mice) shows increased levels of GluN2B ($p<0.05$) and GluN1 ($p<0.01$) relative to WT. There is no change in GluN2A ($p=0.49$) and CaMKII ($p=0.41$). **(C, D)** Total homogenate (n=4 preps/4 mice) signal shows increased levels of GluN2B ($p<0.01$) relative to WT. There is no change in GluN2A ($p=0.41$), GluN1 ($p=0.50$), and CaMKII ($p=0.074$). **(E, F)** Immunoprecipitation of CaMKII from P20 SRKO hippocampi (n=3 preps/ 3 mice) shows decreased CaMKII-GluN2B interaction ($p<0.05$) and

pT286 levels of CaMKII ($p<0.05$) relative to WT. Data are represented as mean +/- SEM. *$p<0.05$; **$p<0.01$; ***$p<0.001$.

**Fig. 4 Enhanced non-ionotropic NMDAR signaling in SRKO mice.**

**(A)** Left: model of the components required for spine growth. Right: schematic of experiment in which the critical components of spine growth that originate from NMDARs are split and $Ca^{2+}$ influx instead comes from VGCCs to observe relative amount of non-ionotropic NMDAR signaling between WT and SRKO. **(B)** Images of spines (yellow arrowhead) before and after HFU+ stimulation (yellow crosshair) in the presence of L689 (10 μM) and Bay K (10 μM) for non-ionotropic NMDAR activation and VGCC-mediated $Ca^{2+}$ influx, respectively. **(C, D)** HFU+ stimulation drives spine growth in WT (black filled circles/bar; n=5 cells/5 mice; $p<0.01$) and SRKO (red filled circles/bar; n=6 cells/4 mice; $p<0.01$), but the amount of growth is larger in SRKO than WT. **(E)** Amplitude of mEPSCs of P15-19 CA1 pyramidal neurons are not changed in SRKO (WT: black line/bar; n=20 cells/3 mice; SRKO red line/bar: n=17 cells/3 mice; $p=0.26$). **(F)** Proposed model. Coincident binding of glutamate and D-serine allows for both non-ionotropic NMDAR signaling and calcium influx required for spine growth. In contrast, reduced levels of D-serine in schizophrenia mouse model SRKO results in glutamate binding alone to more NMDARs in the absence of D-serine that allows for strong non-ionotropic NMDAR activation with small calcium influx that promotes spine shrinkage. Data are represented as mean +/- SEM. *$p<0.05$; **$p<0.01$; ***$p<0.001$.

# Figure 1

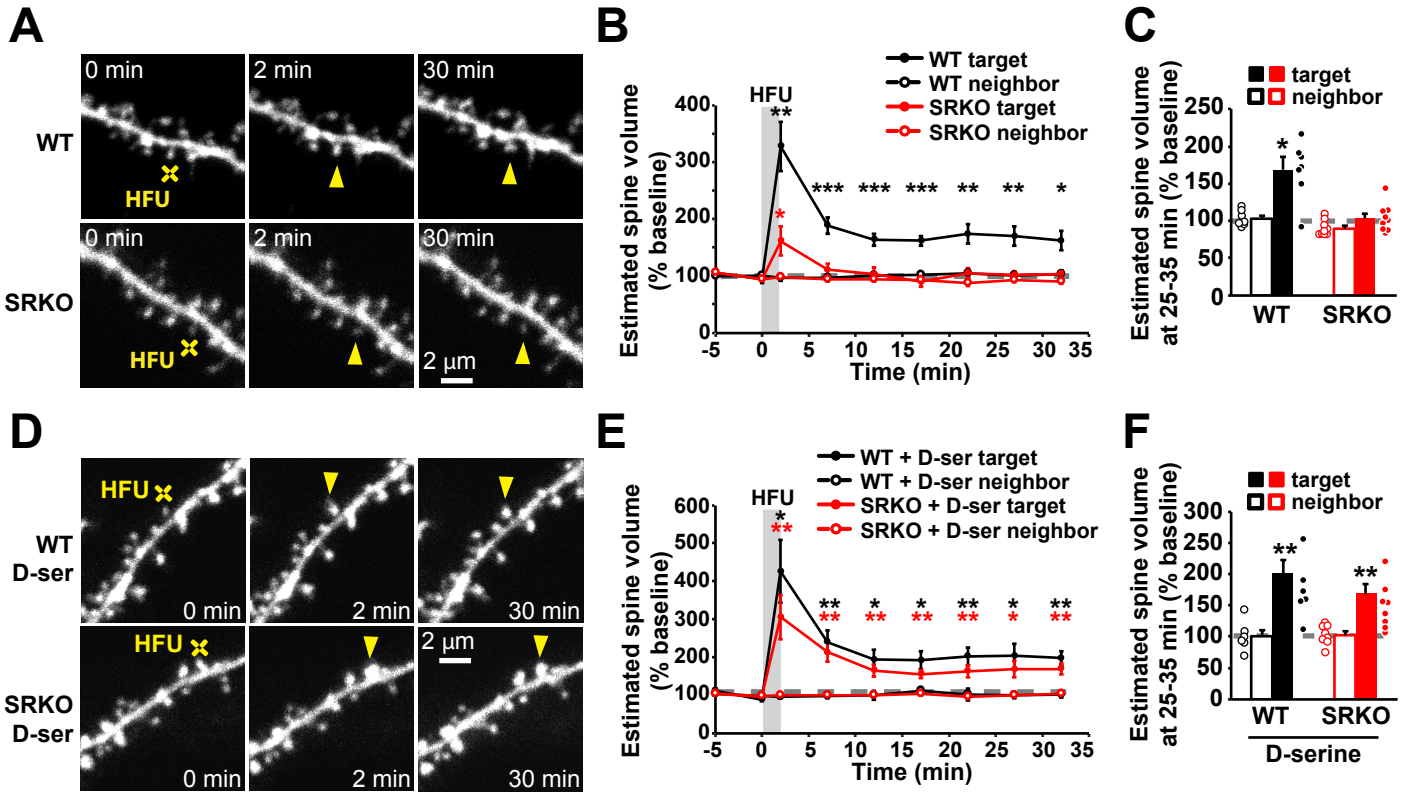
A
WT
SRKO
0 min
2 min
30 min
HFU
2 µm
B
WT target
WT neighbor
SRKO target
SRKO neighbor
HFU
Estimated spine volume (% baseline)
Time (min)
C
target
neighbor
Estimated spine volume at 25-35 min (% baseline)
WT
SRKO
D
WT D-ser
SRKO D-ser
E
WT + D-ser target
WT + D-ser neighbor
SRKO + D-ser target
SRKO + D-ser neighbor
F
D-serine

# Figure 2

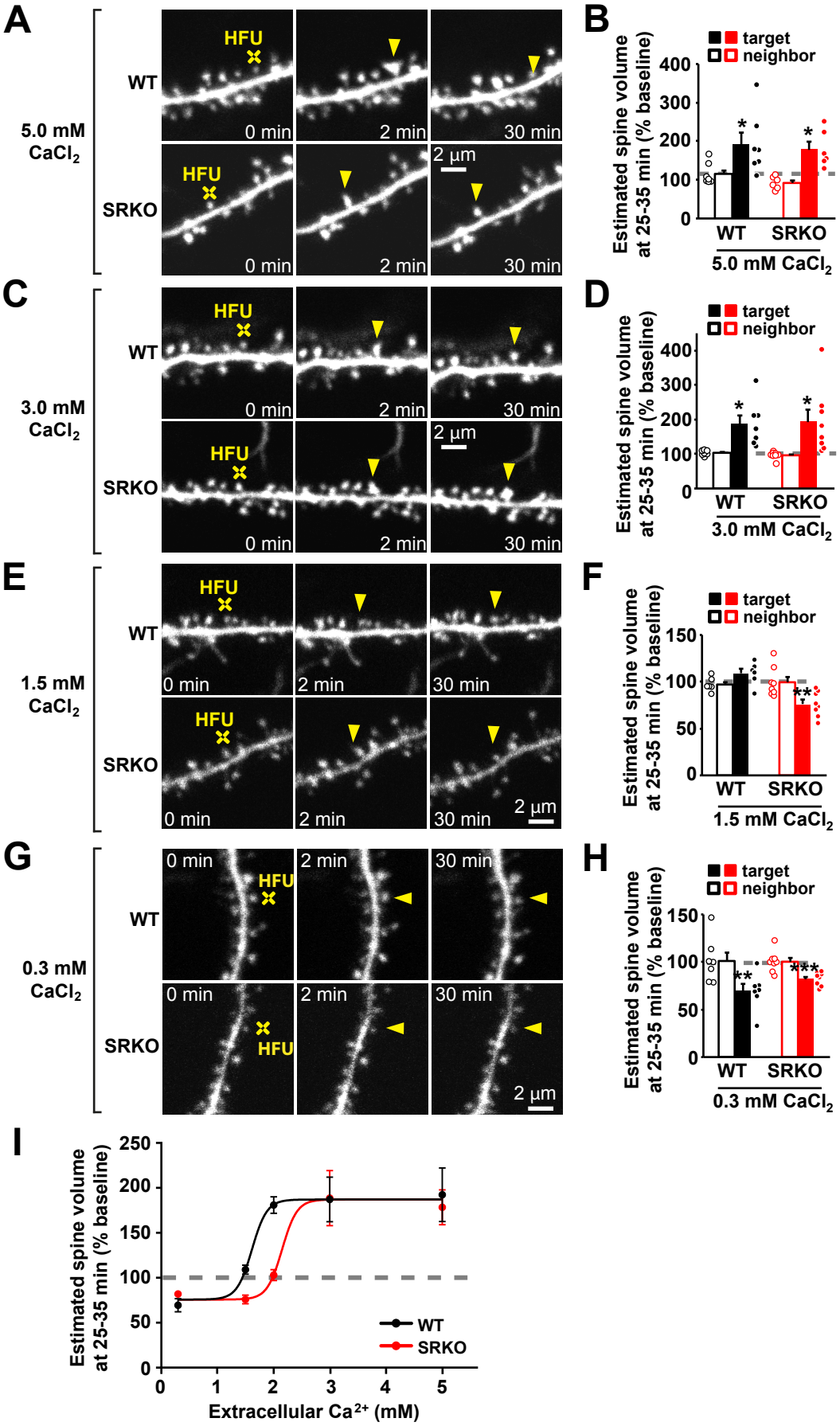
A
5.0 mM CaCl2
WT
SRKO
HFU
0 min
2 min
30 min
2 µm
B
target
neighbor
Estimated spine volume at 25-35 min (% baseline)
WT
SRKO
5.0 mM CaCl2
C
3.0 mM CaCl2
D
3.0 mM CaCl2
E
1.5 mM CaCl2
F
1.5 mM CaCl2
G
0.3 mM CaCl2
H
0.3 mM CaCl2
I
Extracellular Ca2+ (mM)

# Figure 3

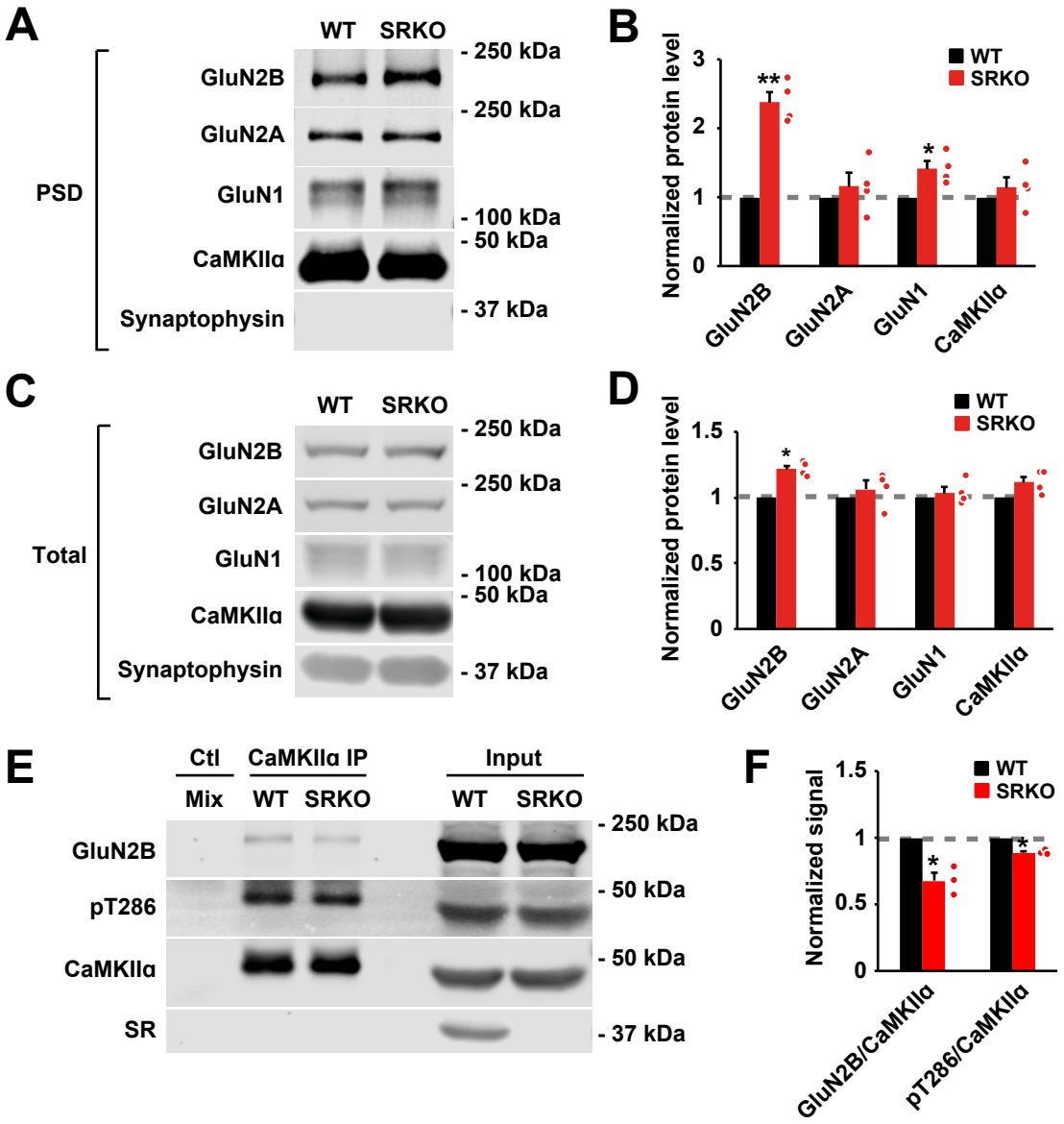
A
WT
SRKO
PSD
GluN2B
GluN2A
GluN1
CaMKIIα
Synaptophysin
- 250 kDa
- 250 kDa
- 100 kDa
- 50 kDa
- 37 kDa
B
Normalized protein level
WT
SRKO
GluN2B
GluN2A
GluN1
CaMKIIα
C
Total
D
E
Ctl
CaMKIIα IP
Input
Mix
pT286
SR
F
Normalized signal
GluN2B/CaMKIIα
pT286/CaMKIIα

# Figure 4

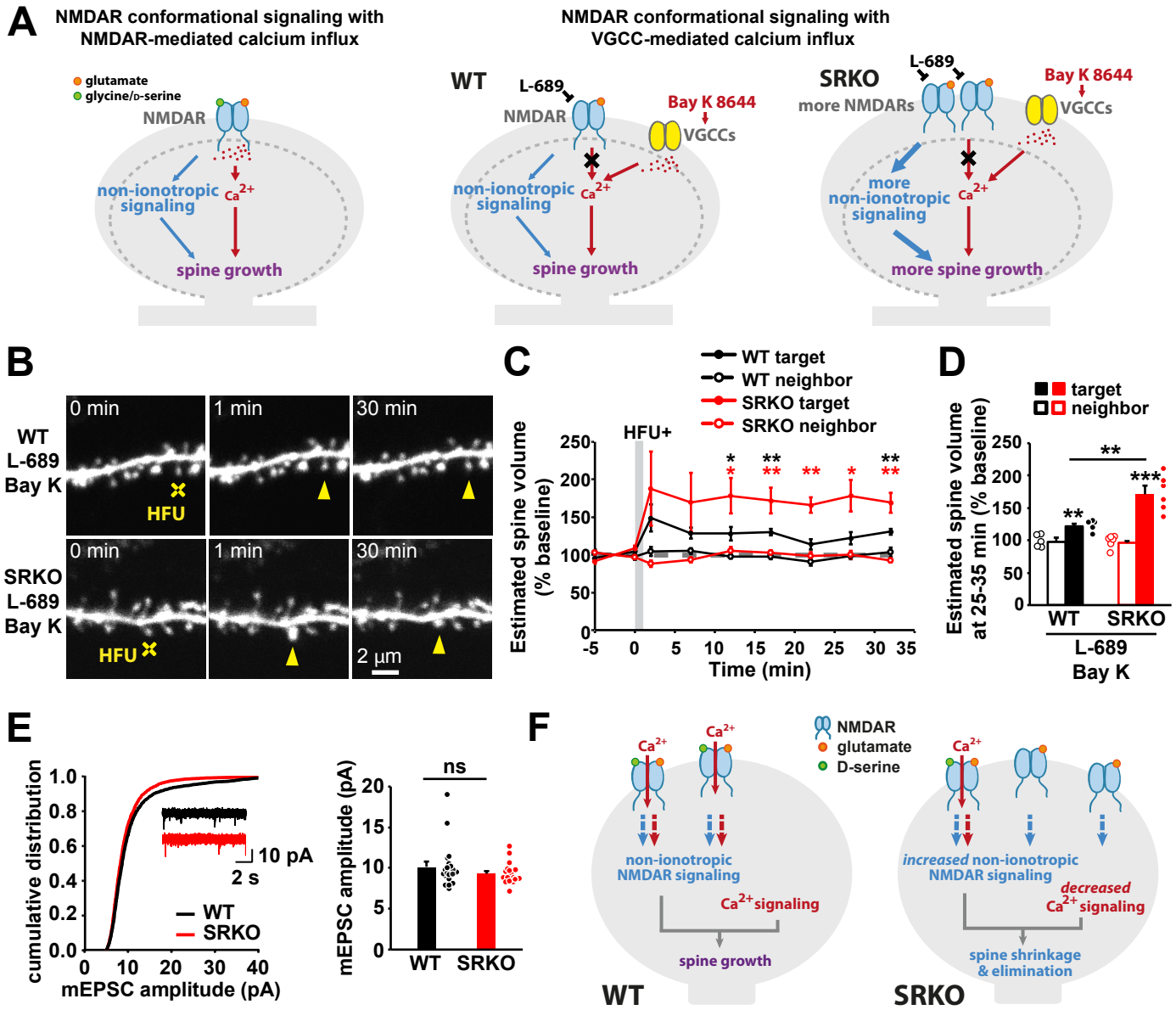
A
NMDAR conformational signaling with NMDAR-mediated calcium influx
glutamate
glycine/D-serine
NMDAR
non-ionotropic signaling
Ca2+
spine growth
NMDAR conformational signaling with VGCC-mediated calcium influx
WT
L-689
NMDAR
Bay K 8644
VGCCs
non-ionotropic signaling
Ca2+
spine growth
SRKO
more NMDARs
L-689
Bay K 8644
VGCCs
more non-ionotropic signaling
Ca2+
more spine growth
B
WT
L-689
Bay K
0 min
1 min
30 min
HFU
SRKO
L-689
Bay K
0 min
1 min
30 min
HFU
2 µm
C
WT target
WT neighbor
SRKO target
SRKO neighbor
HFU+
Estimated spine volume (% baseline)
Time (min)
D
target
neighbor
Estimated spine volume at 25-35 min (% baseline)
WT
SRKO
L-689
Bay K
E
cumulative distribution
mEPSC amplitude (pA)
10 pA
2 s
WT
SRKO
mEPSC amplitude (pA)
ns
WT
SRKO
F
NMDAR
glutamate
D-serine
Ca2+
non-ionotropic NMDAR signaling
Ca2+signaling
spine growth
WT
increased non-ionotropic NMDAR signaling
decreased Ca2+ signaling
spine shrinkage & elimination
SRKO